

Electrical Charge Control of h -BN Single Photon Sources

Mihyang Yu^{1,2}, Donggyu Yim², Hosung Seo², Jieun Lee^{1,2}*

¹Institute of Applied Physics and Department of Physics and Astronomy, Seoul National University, Seoul, 08826, Korea, ²Department of Physics and Department of Energy Systems Research, Ajou University, Suwon, 16499, Korea.

* To whom correspondence should be addressed, lee.jieun@snu.ac.kr.

Abstract

Colour centres of hexagonal boron nitride (h -BN) have been discovered as promising and practical single photon sources due to their high brightness and narrow spectral linewidth at room-temperature. In order to realize h -BN based photonic quantum communications, the ability to electrically activate the single photon fluorescence using an external electric field is crucial. In this work, we show the electrical switching of the photoluminescence from h -BN quantum emitters, enabled by the controllable electron transfer from the nearby charge reservoir. By tuning the Fermi level of graphene next to the h -BN defects, we observed luminescence brightening of a quantum emitter upon the application of a voltage due to the direct charge state manipulation. In addition, the correlation measurement of the single photon sources with the graphene's Raman spectroscopy allows us to extract the exact charge transition level of quantum emitters, providing the information on the crystallographic nature of the defect structure. With the complete on-off switching of emission intensity of h -BN quantum emitters using a voltage, our result paves the way for the van der Waals colour centre based photonic quantum information processing, cryptography and memory applications.

Keywords: Single photon sources, Hexagonal boron nitride, Charge transfer, van der Waals heterostructures

1. Introduction

Hexagonal boron nitride (h -BN) is a two-dimensional (2D) crystal, which has a great potential for the development of novel nanoscale devices [1–3] because of its excellent optical, electrical, thermal and mechanical properties. Due to its ultra-flat surface, high thermal stability and wide band gap (~ 6 eV), h -BN has been useful as ingredients for van der Waals devices such as quantum capacitors, field effect and tunneling transistors, and various quantum optoelectronic devices [4–7]. More recently, h -BN has been found to host defect-derived single photon sources that can generate stable and bright single photon even at room temperature, introducing h -BN as an emerging material platform for the solid-state quantum

information technologies [8,9]. Various progresses have been made to study the nature of the quantum emitters including the identification of the emitter’s crystallographic structure [10–13], their optical characterization [14–17], and the external control of the emission properties [18,19]. Moreover, the artificial device geometries were developed by employing the unique planar nature of *h*-BN such as the localized creation of quantum emitters on prepatterned substrates [20] and coupling *h*-BN emitters with nano-photonic structures [21].

For the exploitation of *h*-BN quantum emitters for quantum communication applications, however, the full electrical manipulation of quantum emitters is highly desired. Although the electrical control of the emitter’s photon energy was achieved in several experiments by applying electric fields to *h*-BN defects [19,22,23], the direct manipulation of the charge state of *h*-BN quantum emitters through a voltage has not been reported yet. By inducing a systematic charge transfer into a quantum defect through a controllable Fermi level manipulation, not only the electrically activated quantum emitters can be achieved, but also information on the defect’s atomic structure identification and charge state dependent luminescence properties can be unveiled [24–26].

In this work, we use graphene as a charge reservoir with a largely tunable Fermi level and negligible emission background [27,28] to induce the direct charge state manipulation of *h*-BN local defects and demonstrate the complete on-off electrical switching of the photoluminescence from *h*-BN quantum emitters. The electrical onset of the *h*-BN defect emission is induced by the Fermi level tuning of the graphene layer, providing the information on the charge transition level of *h*-BN defects, which agrees well with a calculated defect model candidate. Also, we observed the voltage-induced peak splitting of a quantum emitter, suggesting the controllable deformation of the second potential well in the excited-state energy surfaces. Our work demonstrating the electrical activation of *h*-BN quantum emission will be advantageous for the development of 2D optoelectronic single photon devices and the van der Waals based quantum communication and information technologies.

2. Results

2.1 Device and electrical characterization

The schematic of the electrical control of the *h*-BN defect photoluminescence in our work is shown in figure 1(a). The atomic defects in *h*-BN crystals are first prepared by thermal annealing of exfoliated *h*-BN (~ 20 nm thick). To induce the systematic charge transfer from graphene to *h*-BN defects, we fabricated heterostructures consisting of graphene/*h*-BN/graphene stacked layers (device schematics in figure 1(b) and images in supplementary figure S1). With the fabricated device, we performed electrical test measurements of graphene electrodes. By scanning the voltage across graphene in the range from -9 to 9 V, the graphene’s Fermi level energy could be tuned by about 500 meV as verified from Raman spectroscopy. The Raman spectra showing the peak shift and narrowing of the graphene G peak are shown in figure 2(e). The charge neutrality point is found at around 1.5 V. The characteristic Kohn anomaly induced Raman shift of graphene near $E_F \approx \pm 100$ meV is observed [29], indicating the clean interface of the fabricated heterostructure and apparent Fermi level tuning of graphene layers. The measured Fermi level also agrees well with the calculation using the geometric and quantum capacitance of graphene electrodes (See Methods). From the detailed measurement of the $I - V$ curve of our device, the Fowler-Nordheim tunnelling is observed (See supplementary figure S2), which is caused by the electric field induced Fermi level tilting, confirming the effective charge doping of quantum defects in *h*-BN crystals [30–32].

2.2 Electrically activated emitter photoluminescence

With the information of the graphene’s Fermi level control, we then performed 2D spatial scanning measurement of the photoluminescence from *h*-BN devices while varying the applied voltage (V) as shown in figure 1(c and d). For this measurement, a continuous-wave 532 nm laser was used as an excitation source and we spatially scanned over the heterostructure to obtain 2D photoluminescence map. When we applied zero voltage to the device ($V = 0$), no luminescence of light was observed in the area that we scanned as shown in figure 1(c). However, when we turned on the external voltage ($V = -6$ V) and scanned over the same area, several localized luminescence of light was observed at different locations. To better display this, we plotted the wavelength dependent 2D photoluminescence map of *h*-BN in figure 1(d). The microscope image of the scanned area is shown in supplementary figure S1. In this area ($3 \mu\text{m} \times 5 \mu\text{m}$), we found 5 electrically activated *h*-BN emitters with wavelength ranging from 550 and 620 nm. By performing larger area scanning measurements to cover the entire device, we found total dozens of electrically activated *h*-BN emitters from this device (Device 1) and another device (Device 2, image in supplementary figure S1). Interestingly, these voltage-induced *h*-BN emitters showed markedly different voltage dependence between emitters which could be categorized into two kinds, *i.e.*, one with symmetric voltage dependence and another with asymmetric voltage dependence, suggesting the existence of different luminescence mechanisms, which are described below.

2.3 Quantum emitter with symmetric voltage dependence

Figure 2(a) shows the electrically activated light emission from a *h*-BN defect centre which exhibits the emission onset at both positive and negative applied voltages. The emission spectrum at the positive, zero, and negative applied voltages are plotted with vertical shifts in figure 2(b). By applying an external voltage, the emission luminescence emerges, revealing the emitter that was otherwise not observable. The voltage-activated quantum emitter also shows the electric field induced Stark shift as a function of an applied voltage, which is similar to the previous result [19]. Also, as we performed the second order correlation function measurement at $V = 7$ V, the emitter exhibited $g^2(0)$ value below 0.5, showing that the emitter is a single photon source (figure 2(c)). Notably, this single photon emitter shows the symmetric voltage dependence of the emission onset, suggesting that the voltage activation is driven by the doping-induced enhancement of the emission efficiency.

The doping-induced emission enhancement can be understood by the saturation effect of the charge trap sites commonly found around solid-state quantum emitters. These charge traps are consisting of nearby local defects or metastable excited states [17,33] which contribute to the reduction of the radiative emission process. By tuning the Fermi level of graphene as shown in figure 2(d), we can saturate the nearby trap sites through the charge doping from the graphene reservoir, bypassing the non-radiative emission channel and enhancing the emission intensity. Such voltage-induced trap site saturation occurs similarly for both positive and negative applied voltages due to the random distribution of the charge trap sites although the threshold voltages may vary slightly. Alternatively, the observed phenomena could also be explained by the photo-doping effect [34–36], but we exclude this possibility since the voltage thresholds for the onset of the luminescence was independent of the pump laser power as observed from a similar emitter (See supplementary figure S3 and S4).

2.4 Quantum emitter with asymmetric voltage dependence

On the other hand, we also observed another type of emitter that exhibits intriguing asymmetric voltage dependence as shown in figure 3(a). In this emitter, the luminescence is switched on only at the negative applied voltage. The detailed measurement spectra are shown in figure 3(b). The second order correlation function measurement also supports that this emitter is a single photon source (figure 3(c)) and the emitted light is found to have a linear polarization (supplementary figure S5). In our experiment, there were several similar emitters that turns on by exerting negative applied voltages, but there also were emitters that shows

up by exerting positive applied voltages. These emitters emerging only at single sign of applied voltages cannot be explained by the trap site saturation effect because of the symmetric geometry of our device structure.

Below, we argue that the emitters with asymmetric voltage dependence originates from the charge transfer process from graphene reservoir to *h*-BN defects, which alters the charge state of quantum defects. Similar like NV^0 and NV^- defect centres in diamond [37,38], *h*-BN quantum emitters could also have different emission energy, spin configuration and brightness depending on the defect's charge state or doping level [19,25,26,37,39–41]. By controllably doping the *h*-BN emitters by graphene charge reservoir, we have shown the change of the emitter's luminescence properties when the Fermi level crosses the charge transition level (CTL) of the *h*-BN defect. Naturally, this charge transition induced emitter switching depends on the applied voltage asymmetrically. By taking into account the band diagram of graphene and *h*-BN (Figure 3(d and e)), we find that at the emitter luminescence threshold voltage (~ -4 V), the measured CTL energy of this quantum emitter is about 4.0 – 4.8 eV above the valence band maximum of *h*-BN. The value is obtained by fully considering the field-induced modification of the band structure (See supplementary figure S6), the exact value of the Fermi level tuning of graphene (upper axis of figure 2(e)), and the depth of quantum emitters embedded beneath the surface of *h*-BN which has the typical range of about 0 – 3 nm [42]. More detailed information on the CTL energy estimation can be found in supplementary figure S7.

Furthermore, above experimental results lead us to identify the crystallographic nature of the observed quantum emitter. Among various defect model candidates in *h*-BN crystal [11,13,43,44], we locate the boron vacancy with dangling bonds (BVDB) [44,45] as a highly possible single photon source which agrees well with our experiment (figure 3(f)). The negatively charged BVDB emitter ($BVDB^-$) is calculated to have a bright zero phonon line (ZPL) emission around 2 eV with two-fold absorption and emission polarization angle dependence. The neutral BVDB emitter ($BVDB^0$), on the other hand, has ZPL energy at 3.27 eV but this emission is weak due to the significant electron-phonon coupling [44]. The calculated CTL energy between $BVDB^-$ and $BVDB^0$ is at 4.8 eV above the valence band maximum of the *h*-BN [44], which is in excellent agreement with our experimental results. From the charge state dependent luminescence properties, our work provides an experimental evidence that $BVDB^-$ is a potential single photon source in *h*-BN crystal and demonstrates its controllable charge state manipulation through a voltage.

2.5 Voltage-induced quantum emitter peak splitting

Lastly, we report the observation of an emitter exhibiting the intriguing voltage-induced emitter peak splitting. Figure 4(a) is the voltage scan result of the emitter, which shows an additional peak at 564 nm appearing at 5 V in the presence of an original peak at 560 nm. The emission polarizations of the two peaks are aligned to the same axis as displayed in figure 4(d). Since the emerging peak has the same polarization with the original peak and the two peaks displayed simultaneous spectral jumps (See supplementary figure S8), we confirm that both peaks originate from the same emitter. The energy difference between the original peak and the emerging peak was about 15 meV and the magnitude of the electric dipole moment of each peak was measured to be 0.065 and 0.26 Debye, respectively. Another emitter with similar properties is also shown in supplementary figure S9.

Such difference in electric dipole moment of the emission peak shift suggests that the two peaks should have been originated from the different crystallographic origin of the same defect. In this regard, we propose the voltage-induced development of a second potential well in the emitter's excited-state adiabatic potential energy surface (APES) as shown in figure 4(e). In the absence of an external voltage, the excited-state has a single-well APES, but it has a meta-stable point close in the configurational coordinate, which is associated with an atomic tilt in the out-of-plane direction, providing extra degrees of freedom to the defects. Upon the application of a voltage, the defect can lower the energy of the meta-stable configuration

owing to the electric-field induced energy shift, associated with the emerging dipole in the out-of-plane direction. As a result, the second ZPL luminescence can be generated through the modified APES. The model is in good agreement with experimental observations since the observed peak splitting energy in experiment is about a few tens of meV. Also, the measured dipole moment of the second ZPL has a significantly larger value than the original one in consistent with the field-induced structural modifications. Moreover, reversing the direction of the electric field will raise the energy of the second potential well, resulting in the asymmetric voltage dependence of the emerging peak. Our observation of electric-field induced level splitting in a single photon source requires further studies to better understand its characteristics, which may lead to the demonstration of the coherent coupling of different states in quantum emitters and the entangled photon pair generation in *h*-BN crystals [46].

3. Conclusions

To conclude, we observed the electrically induced photon emission switching and level splitting in *h*-BN quantum emitters by controlling the Fermi level tuning of graphene. The complete turn on of the emitter luminescence beyond the threshold voltage in bidirectional and unidirectional applied voltage is found to be originated from the electrical control of the nearby charge trap sites and the direct charge state manipulation of the defect centre ($BVDB^- \leftrightarrow BVDB^0$), respectively. The voltage-induced activation of the peak splitting was also observed which is explained by the formation of the second potential well in the excited-state potential energy surfaces. Such remarkable on/off control of emitter luminescence using a voltage will be useful for the optoelectronic single photon device developments, opening a route towards 2D chip-based solid-state quantum information processing and communications.

Methods

Sample preparation

h-BN crystal (HQ graphene) was mechanically exfoliated onto SiO₂/Si substrates by using scotch tapes to obtain thin flakes. Exfoliated *h*-BN flakes were rinsed in acetone for 10 mins and in isopropyl alcohol (IPA) for 5 mins to remove tape residues. Then *h*-BN flakes were thermally annealed for 2 h at 800 °C under the condition of argon gas flow (1 Torr) to create optically active *h*-BN defects. For the preparation of graphene electrodes, monolayer and bilayer graphene were obtained through mechanical exfoliation from graphite. We used a dry transfer method using polycarbonate (PC) film to fabricate graphene/*h*-BN/graphene stacks which are transferred directly onto SiO₂/Si substrates with prepatterned Au electrodes. PC residue was then sequentially removed by dipping the sample in chloroform for 8 h, acetone for 30 mins, and IPA for 30 mins.

Optical measurements

In the optical confocal microscopy setup, a 532 nm solid-state continuous-wave (cw) laser was incident onto the sample through an objective lens (NA = 0.6). The emitted light was collected using the same objective and reflected at a beam splitter and guided to a spectrometer with CCD detector. XY-piezostages inside a cryostat were used to move the sample position to perform 2D spatial scanning. The excitation and emission polarization dependent measurement of emitters was performed by rotating a half-wave plate (HWP) between the sample and a polarizer in the excitation and collection path, respectively. The polar plot of the polarization dependent emission intensity data was fitted by using $\cos^2(\theta)$ function, where $\theta/2$ is the HWP rotation angle.

For the second order correlation measurement, we placed a flip mirror in front of the spectrometer to guide the optical path to the Hanbury Brown and Twiss (HBT) interferometer. In this path, additional bandpass filters were used to spectrally purify the defect luminescence. The emitted light from *h*-BN defect was split by a 50:50 beam splitter and detected by two single-photon counting modules (SPCM). Electrical signals from SPCMs were processed by a time-correlated single-photon counting device (TCSPC) to obtain the second order correlation data, $g^2(\tau)$, as a function of the time delay (τ). $g^2(\tau)$ curve was fitted by $g^2(\tau) = 1 - \alpha e^{-|\tau/\tau_1|}$, where α is a fitting parameter ($0 \leq \alpha \leq 1$) and τ_1 is the emission lifetime of the defect.

Raman spectroscopy is performed to monitor the Fermi level tuning of graphene electrodes. A 532 nm cw laser was used as an excitation source with power below 200 μ W. We focused on the graphene Raman G peak which shows the spectral shift and narrowing as a function of the carrier concentration to extract the graphene's Fermi level tuning while applying voltages [47].

Fermi level tuning calculation

To calculate the Fermi level tuning of the graphene electrode (ΔE_F) as a function of an applied voltage (V), we use the following relation [47,48]

$$eV = \Phi + 2\Delta E_F = e \left(\frac{en_{Gr}}{C_{Gr}} \right) + 2\Delta E_F$$

where Φ is the energy offset between the Dirac point of two graphene and ΔE_F is the Fermi level shift of the graphene at the Dirac point. The first term comes from the geometric capacitance of the graphene using $C_{Gr} = \frac{\epsilon_0 \epsilon_{BN}}{t_{BN}}$, where ϵ_0 , ϵ_{BN} , and t_{BN} are the vacuum permittivity, relative permittivity of *h*-BN, and the thickness of *h*-BN, respectively. The second term is attributed to the quantum capacitance of each graphene electrode. Since the charge concentration of graphene can be calculated by $n_{Gr} = \int_{min}^{max} \rho_{Gr}(E) dE$ where $\rho_{Gr}(E)$ is the density of state and $\rho_{Gr}(E) = \frac{E}{\pi \hbar^2 v_F^2}$, we get $n_{Gr} = \frac{\Delta E_F^2}{\pi \hbar^2 v_F^2}$. Here \hbar and v_F are the Plank constant and Fermi velocity, respectively. Finally the relation between the Fermi level tuning and the applied voltage is given by

$$eV = \frac{e^2}{\pi \hbar^2 v_F^2} \frac{t_{BN}}{\epsilon_0 \epsilon_{BN}} \Delta E_F^2 + 2\Delta E_F.$$

Applying above relations to our experimental results, the voltage tuning range in the Device 1 from -9 to 9 V yields the range of the Fermi level shift over the range of about 500 meV (See supplementary figure S8). This range is consistent with the independent measurement of the graphene's Fermi level tuning obtained by Raman spectroscopy (figure 2(e)) [29].

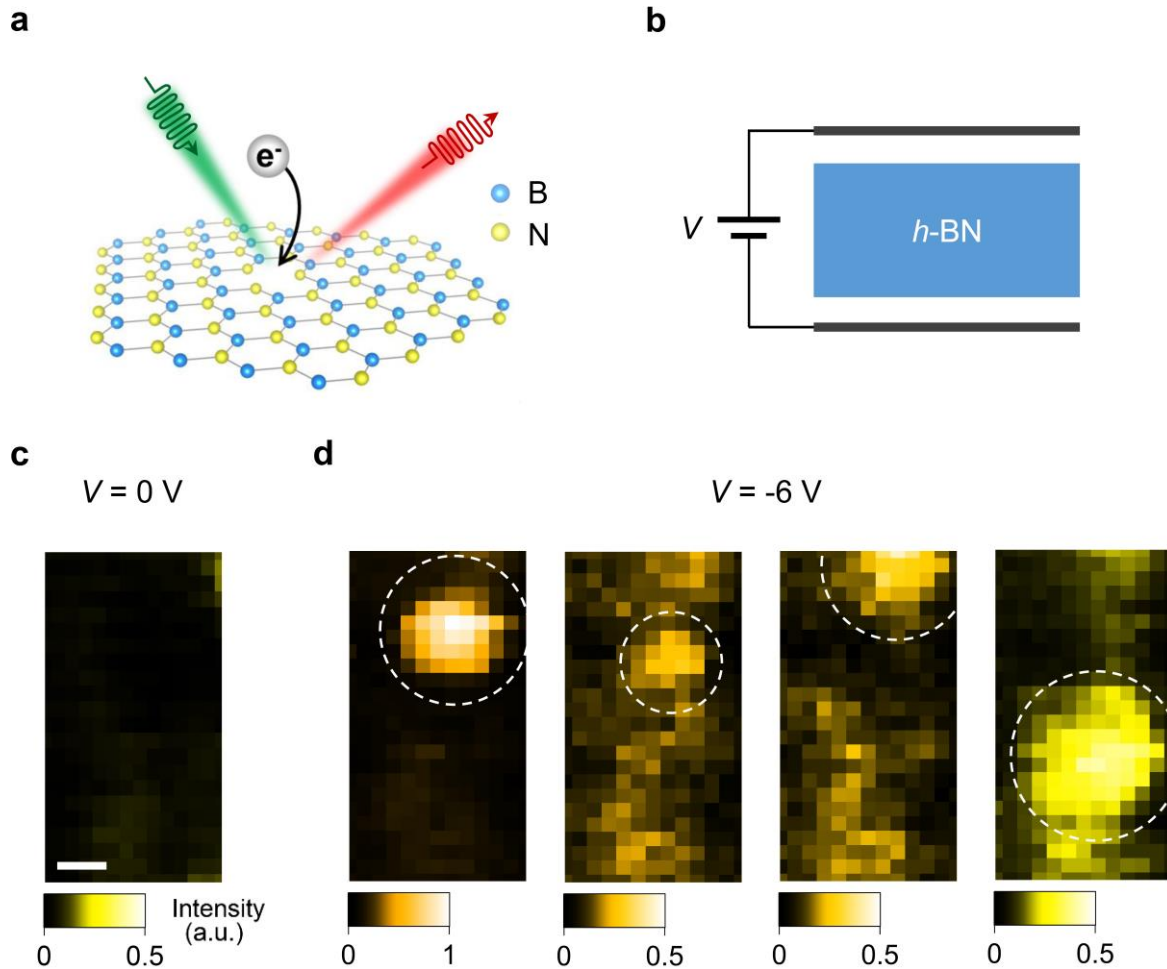


Figure 1 Electrical switching of *h*-BN emitter photoluminescence. (a) Schematics of the photoluminescence of electrically doped *h*-BN local defect. Green and red coloured rays indicate excitation laser and emitted light, respectively. B: boron. N: nitrogen. (b) Device schematics of graphene-stacked *h*-BN heterostructure. (c) 2D photoluminescence scan image of *h*-BN device measured in the absence of an applied voltage. Scale bar: 1 μm . (d) 2D scan image upon the application of an external voltage of -6 V, showing the localized photon emission. The positions of the localized emitters are indicated by white dashed lines. Emission intensity maps are shown for the wavelength at 616, 609, 605, and 584 nm from left to right panels, respectively.

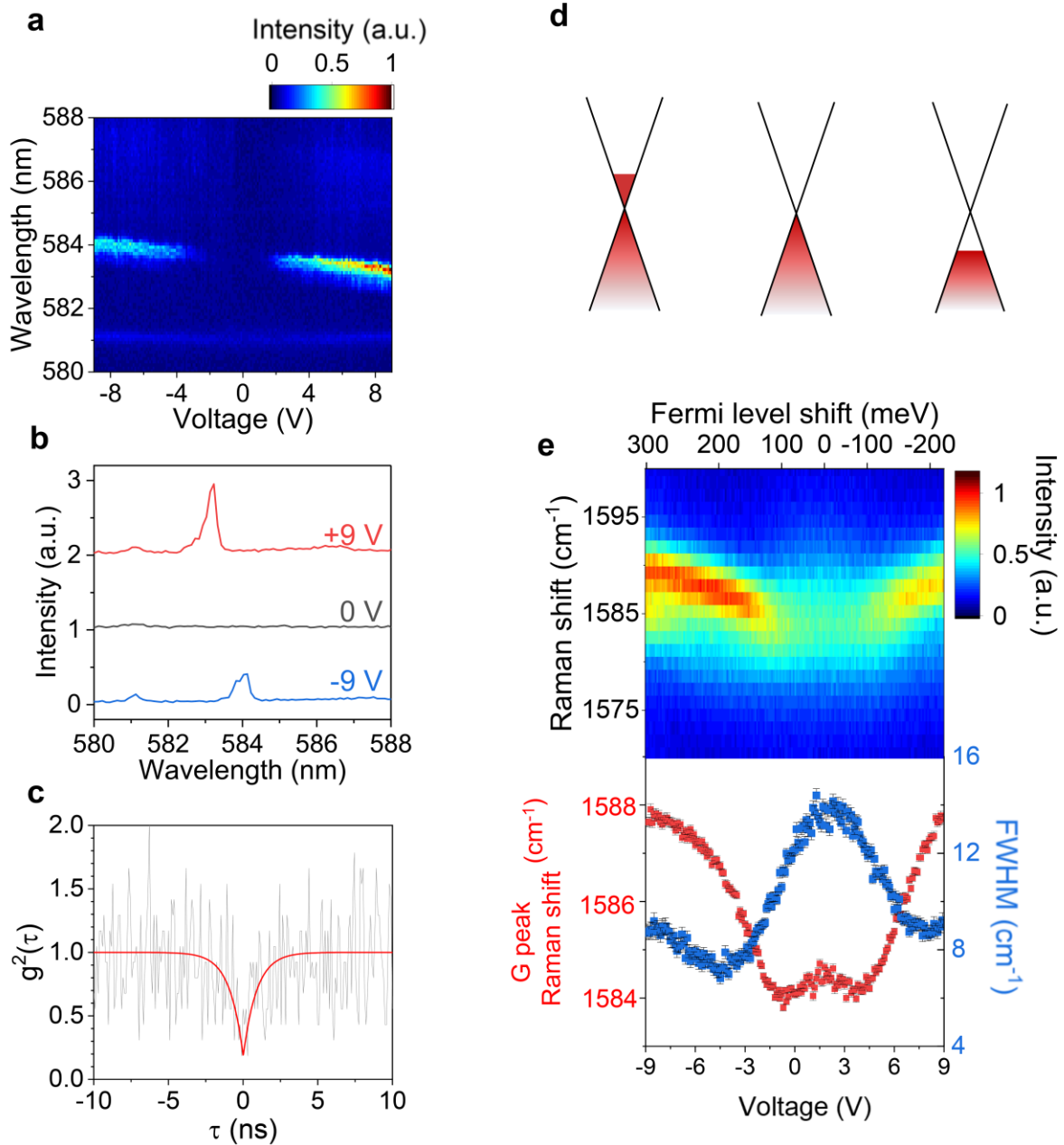


Figure 2. Emitter with symmetric voltage dependence and correlation with the graphene's Raman measurement. (a) Colour plot of the voltage-activated emitter intensity as functions of the wavelength and applied voltage. (b) Emission spectrum at 9 V (red), 0 V (black), and -9 V (blue). Spectral lines are vertically shifted. (c) The second order correlation function measured at 7 V, showing that the emitter is a single photon source. The black line is the measurement data and the red line is the fitting result using the following parameters: $g^2(0) = 0.183$ and $\tau_1 = 900$ ps. (d) Fermi level tuning of graphene for negative (left), zero (centre), and positive (right) applied voltages. (e) (Upper) Spectra of graphene G Raman peak as a function of the applied voltage. (Lower) Raman center peak position (red square) and full width at half maximum (FWHM) (blue square) obtained by Lorentzian fit functions. Fitting error bars are shown together.

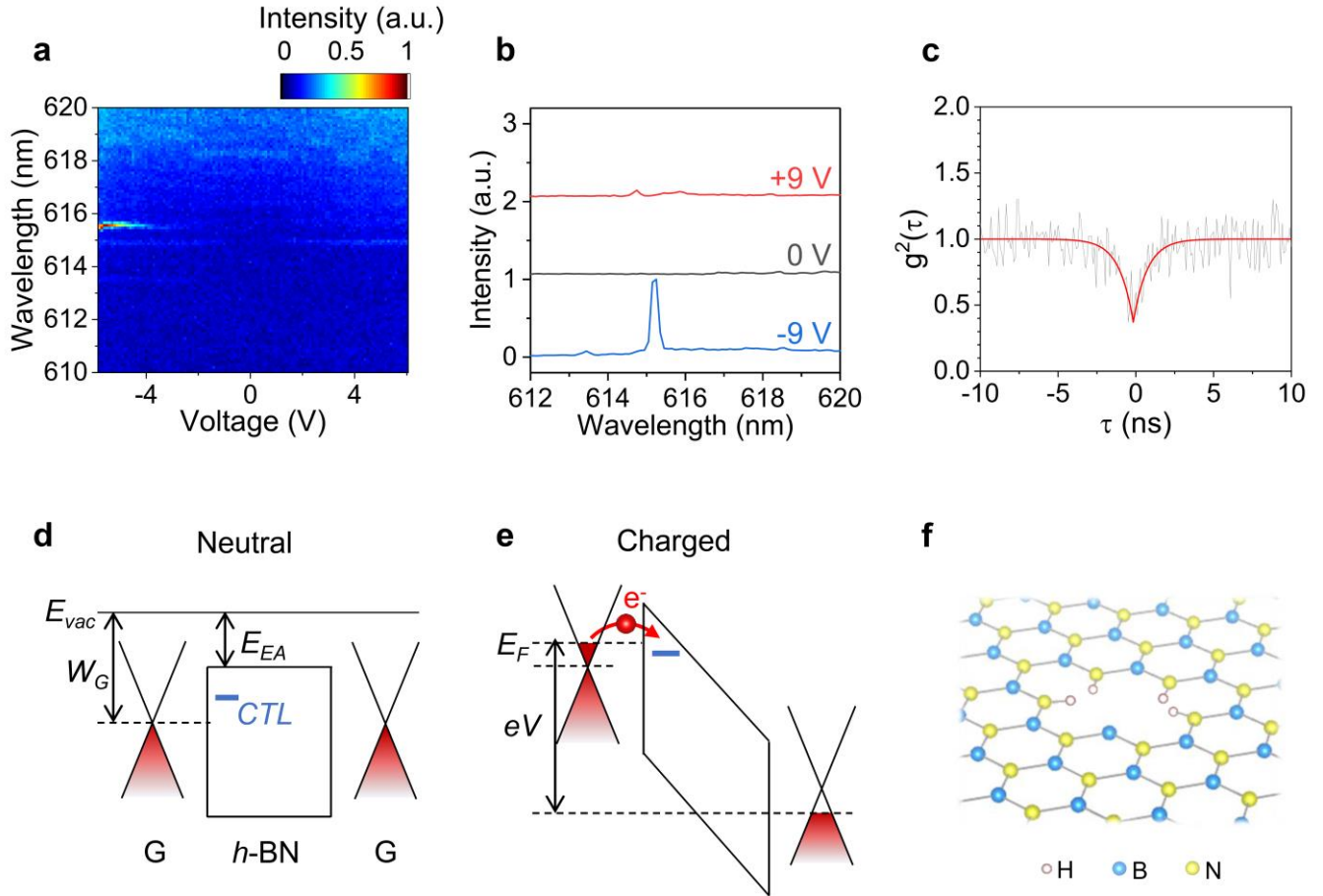


Figure 3. Emitter with asymmetric voltage dependence and the charge transition of *h*-BN single photon source. (a) Colour plot of the voltage-activated emitter intensity as functions of the wavelength and applied voltage. (b) Emission spectrum at 9 V (red), 0 V (black), and -9 V (blue). Spectral lines are vertically shifted. (c) The second order correlation function measured at -9 V, showing that the emitter is a single photon source. The black line is the measurement data and the red line is the fitting result using the following parameters: $g^2(0) = 0.372$ and $\tau_1 = 898$ ps. (d) Band diagram of the heterostructure in the absence of an external voltage. E_{vac} : Vacuum energy level. W_G : Work function of neutral graphene (~ 4.5 eV). E_{EA} : Electron affinity of *h*-BN (~ 2.3 eV). CTL: Charge transition level of *h*-BN quantum defect. (e) Band diagram when an external voltage (V) charges the *h*-BN quantum defect. Electron is transferred from graphene to *h*-BN emitter. (f) Crystal structure of a quantum emitter candidate model, boron vacancy with dangling bonds (BVDB), which has the CTL energy similar to experimental results. H: hydrogen. B: boron. N: nitrogen.

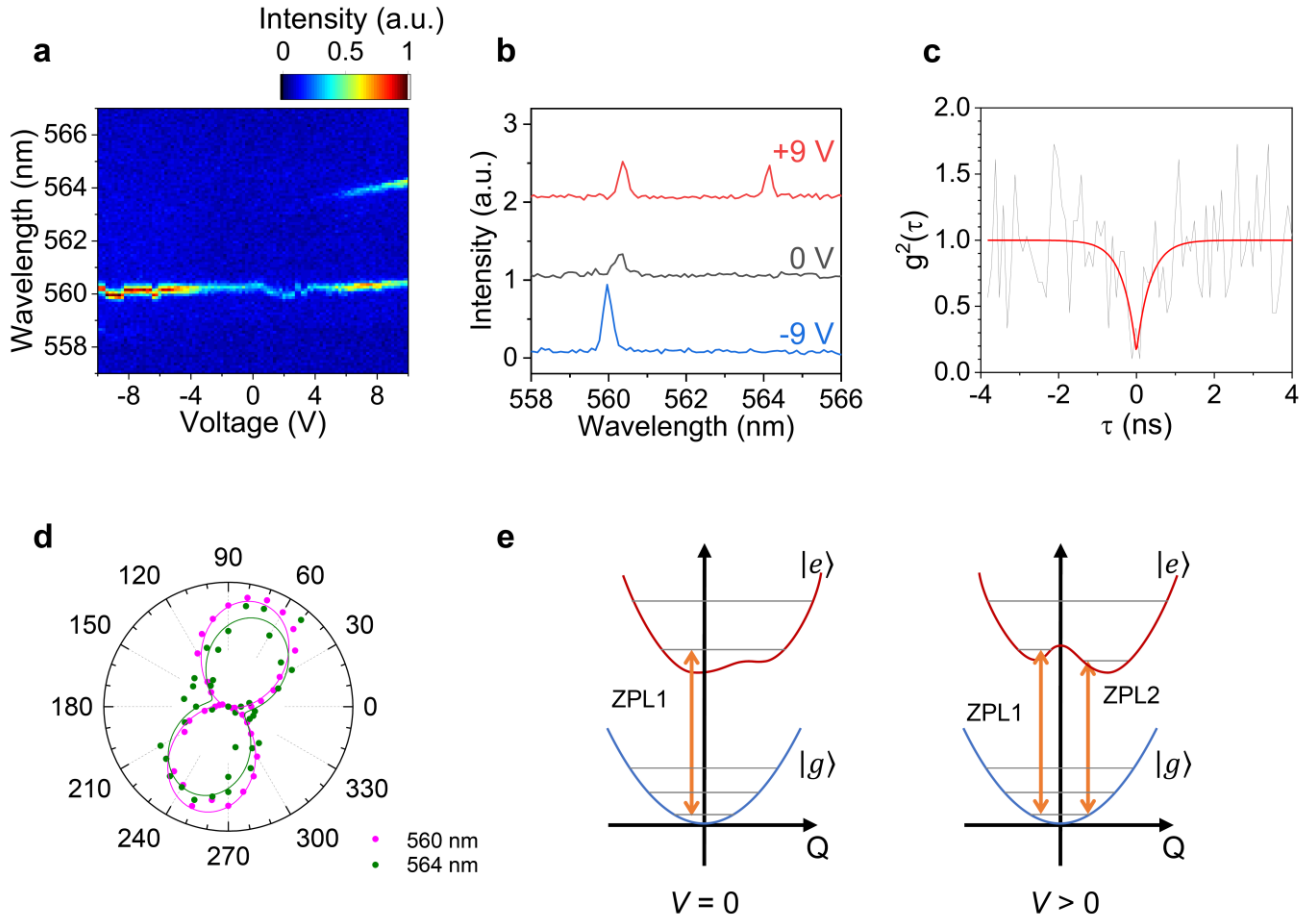


Figure 4. Voltage-induced level splitting of *h*-BN emitter. (a) Colour plot of the emitter peak intensities as functions of the wavelength and applied voltage. (b) Emission spectrum at 9 V (red), 0 V (black), and -9 V (blue). Spectral lines are vertically shifted. (c) The second order correlation function measured at -6 V, showing that the emitter is a single photon source. The black line is the measurement data and the red line is the fitting result using the following parameters: $g^2(0) = 0.150$ and $\tau_1 = 355$ ps. (d) Polar plots of the emission polarization dependence of the peak at 560 nm (magenta) and 564 nm (green), displaying almost the same polarization orientation. (e) Configurational coordinate diagrams depicting the evolution of the excited-state potential energy surface as a function of an external voltage. (Left) In the absence of an external voltage, one zero-phonon line (ZPL1) is possible, but there is a meta-stable point in the proximity of the excited-state zero-phonon vibrational state. (Right) Applying an external voltage beyond threshold, a second potential well is formed, providing the second zero-phonon luminescence channel (ZPL2). Q : configurational coordinate. $|g\rangle$: ground state energy. $|e\rangle$: excited state energy.

References

- [1] Dean C R *et al.* 2010 Boron nitride substrates for high-quality graphene electronics *Nat. Nanotechnol.* **5** 722
- [2] Mayorov A S *et al.* 2011 Micrometer-scale ballistic transport in encapsulated graphene at room temperature *Nano Lett.* **11** 2396
- [3] Wang L, Chen Z, Dean C R, Taniguchi T, Watanabe K, Brus L E and Hone J 2012 Negligible environmental sensitivity of graphene in a hexagonal boron nitride/graphene/h-BN sandwich structure *ACS Nano* **6** 9314
- [4] Cassabois G, Valvin P and Gil B 2016 Hexagonal boron nitride is an indirect bandgap semiconductor *Nat. Photonics* **10** 262
- [5] Yu G L *et al.* 2013 Interaction phenomena in graphene seen through quantum capacitance *Proc. Natl. Acad. Sci. U. S. A.* **110** 3282
- [6] Britnell L *et al.* 2012 Field-effect tunneling transistor based on vertical graphene heterostructures *Science* **335** 947
- [7] Withers F *et al.* 2015 WSe₂ light-emitting tunneling transistors with enhanced brightness at room temperature *Nano Lett.* **15** 8223
- [8] Tran T T, Bray K, Ford M J, Toth M and Aharonovich I 2016 Quantum emission from hexagonal boron nitride monolayers *Nat. Nanotechnol.* **11** 37
- [9] Dietrich A, Doherty M W, Aharonovich I and Kubanek A 2020 Solid-state single photon source with Fourier transform limited lines at room temperature *Phys. Rev. B* **101** 081401
- [10] Tawfik S A, Ali S, Fronzi M, Kianinia M, Tran T T, Stampfl C, Aharonovich I, Toth M and Ford M J 2017 First-principles investigation of quantum emission from hBN defects *Nanoscale* **9** 13575
- [11] Abdi M, Chou J P, Gali A and Plenio M B 2018 Color centers in hexagonal boron nitride monolayers: a group theory and ab initio analysis *ACS Photonics* **5** 1967
- [12] Sajid A, Reimers J R and Ford M J 2018 Defect states in hexagonal boron nitride: assignments of observed properties and prediction of properties relevant to quantum computation *Phys. Rev. B* **97** 064101
- [13] Sajid A and Thygesen K S 2020 VN₂C₂B defect as source of single photon emission from hexagonal boron nitride *2D Mater.* **7** 031007
- [14] Schell A W, Tran T T, Takashima H, Takeuchi S and Aharonovich I 2016 Non-linear excitation of quantum emitters in hexagonal boron nitride multilayers *APL Photonics* **1** 091302
- [15] Exarhos A L, Hopper D A, Grote R R, Alkauskas A and Bassett L C 2017 Optical signatures of quantum emitters in suspended hexagonal boron nitride *ACS Nano* **11** 3328
- [16] Yim D, Yu M, Noh G, Lee J and Seo H 2020 Polarization and localization of single-photon emitters in hexagonal boron nitride wrinkles *ACS Appl. Mater. Interfaces* **12** 36362
- [17] Boll M K, Radko I P, Huck A and Andersen U L 2020 Photophysics of quantum emitters in hexagonal boron-nitride nano-flakes *Opt. Express* **28** 7475
- [18] Grosso G, Moon H, Lienhard B, Ali S, Efetov D K, Furchi M M, Jarillo-Herrero P, Ford M J, Aharonovich I and Englund D 2017 Tunable and high-purity room temperature single-photon emission from atomic defects in hexagonal boron nitride *Nat. Commun.* **8** 705
- [19] Noh G, Choi D, Kim J H, Im D G, Kim Y H, Seo H and Lee J 2018 Stark tuning of single-photon emitters in hexagonal boron nitride *Nano Lett.* **18** 4710
- [20] Fournier C *et al.* 2021 Position-controlled quantum emitters with reproducible emission wavelength in hexagonal boron nitride *Nat. Commun.* **12** 3779
- [21] Fröch J E, Kim S, Mendelson N, Kianinia M, Toth M and Aharonovich I 2020 coupling hexagonal boron nitride quantum emitters to photonic crystal cavities *ACS Nano* **14** 7085
- [22] Scavuzza A, Mangel S, Park J H, Lee S, Loc Duong D, Strelow C, Mews A, Burghard M and Kern K 2019 Electrically tunable quantum emitters in an ultrathin graphene-hexagonal boron nitride van der Waals heterostructure *Appl. Phys. Lett.* **114** 062104
- [23] Mendelson N, Xu Z Q, Tran T T, Kianinia M, Scott J, Bradac C, Aharonovich I and Toth M 2019 Engineering and tuning of quantum emitters in few-layer hexagonal boron nitride *ACS Nano* **13** 3132
- [24] Wolfowicz G, Heremans F J, Anderson C P, Kanai S, Seo H, Gali A, Galli G and Awschalom D D 2021 Quantum guidelines for solid-state spin defects *Nat. Rev. Mater.* **6** 906
- [25] Anderson C P *et al.* 2019 Electrical and optical control of single spins integrated in scalable semiconductor devices *Science* **366** 1225
- [26] Widmann M *et al.* 2019 Electrical Charge state manipulation of single silicon vacancies in a silicon carbide quantum optoelectronic device *Nano Lett.* **19** 7173
- [27] Nair R R, Blake P, Grigorenko A N, Novoselov K S, Booth T J, Stauber T, Peres N M R and Geim A K 2008 Fine structure constant defines visual transparency of graphene *Science* **320** 1308
- [28] Wong D *et al.* 2015 Characterization and manipulation of individual defects in insulating hexagonal boron nitride using scanning tunnelling microscopy *Nat. Nanotechnol.* **10** 949

- [29] Yan J, Henriksen E A, Kim P and Pinczuk A 2008 Observation of anomalous phonon softening in bilayer graphene *Phys. Rev. Lett.* **101** 136804
- [30] Britnell L *et al.* 2012 Electron tunneling through ultrathin boron nitride crystalline barriers *Nano Lett.* **12** 1707
- [31] Lee S H, Choi M S, Lee J, Ho Ra C, Liu X, Hwang E, Choi J H, Zhong J, Chen W and Yoo W J 2014 High performance vertical tunneling diodes using graphene/hexagonal boron nitride/graphene hetero-structure *Appl. Phys. Lett.* **104** 053103
- [32] Greenaway M T, Vdovin E E, Ghazaryan D, Misra A, Mishchenko A, Cao Y, Wang Z, Wallbank J R, Holwill M, Khanin Y N *et al.* 2018 Tunnel spectroscopy of localised electronic states in hexagonal boron nitride *Commun. Phys.* **1** 94
- [33] Neitzke O, Morfa A, Wolters J, Schell A W, Kewes G and Benson O 2015 Investigation of line width narrowing and spectral jumps of single stable defect centers in ZnO at cryogenic temperature *Nano Lett.* **15** 3024
- [34] Khatri P, Ramsay A J, Malein R N E, Chong H M H and Luxmoore I J 2020 Optical gating of photoluminescence from color centers in hexagonal boron nitride *Nano Lett.* **20** 4256
- [35] White S J U, Duong N M H, Solntsev A S, Kim J H, Kianinia M and Aharonovich I 2020 Optical repumping of resonantly excited quantum emitters in hexagonal boron nitride *Phys. Rev. Appl.* **14** 044017
- [36] Kianinia M *et al.* 2018 All-optical control and super-resolution imaging of quantum emitters in layered materials *Nat. Commun.* **9** 874
- [37] Grotz B *et al.* 2012 Charge state manipulation of qubits in diamond *Nat. Commun.* **3** 729
- [38] Karaveli S, Gaathon O, Wolcott A, Sakakibara R, Shemesh O A, Peterka D S, Boyden E S, Owen J S, Yuste R and Englund D 2016 Modulation of nitrogen vacancy charge state and fluorescence in nanodiamonds using electrochemical potential *Proc. Natl. Acad. Sci. U. S. A.* **113** 3938
- [39] De Las Casas C F, Christle D J, Ul Hassan J, Ohshima T, Son N T and Awschalom D D 2017 Stark tuning and electrical charge state control of single divacancies in silicon carbide *Appl. Phys. Lett.* **111** 262403
- [40] Brotons-Gisbert M, Branny A, Kumar S, Picard R, Proux R, Gray M, Burch K S, Watanabe K, Taniguchi T and Gerardot B D 2019 Coulomb blockade in an atomically thin quantum dot coupled to a tunable Fermi reservoir *Nat. Nanotechnol.* **14** 442
- [41] Chakraborty C, Kinnischtzke L, Goodfellow K M, Beams R and Vamivakas A N 2015 Voltage-controlled quantum light from an atomically thin semiconductor *Nat. Nanotechnol.* **10** 507
- [42] Vogl T, Doherty M W, Buchler B C, Lu Y and Lam P K 2019 Atomic localization of quantum emitters in multilayer hexagonal boron nitride *Nanoscale* **11** 14362
- [43] Mendelson N *et al.* 2021 Identifying carbon as the source of visible single-photon emission from hexagonal boron nitride *Nat. Mater.* **20** 321
- [44] Turiansky M E, Alkauskas A, Bassett L C and Van De Walle C G 2019 Dangling bonds in hexagonal boron nitride as single-photon emitters *Phys. Rev. Lett.* **123** 127401
- [45] Turiansky M E and van de Walle C G 2021 Impact of dangling bonds on properties of h-BN *2D Mater.* **8** 024002
- [46] Bennett A J *et al.* 2010 Electric-field-induced coherent coupling of the exciton states in a single quantum dot *Nat. Phys.* **6** 947
- [47] Das A, Chakraborty B, Piscanec S, Pisana S, Sood A K and Ferrari A C 2009 Phonon renormalization in doped bilayer graphene *Phys. Rev. B* **79** 155417
- [48] Kuzmina A, Parzefall M, Back P, Taniguchi T, Watanabe K, Jain A and Novotny L 2021 Resonant light emission from graphene/hexagonal boron nitride/graphene tunnel junctions *Nano Lett.* **21** 8332